Determination of the Σ 21 [211] orientational relationship in a MgO/Cu composite

Wang, Y.G.; Yan, G.H.; Hosson, J.Th.M. De

Published in:
Materials Science and Engineering%3A A

DOI:
10.1016/S0921-5093(01)01229-1

Publication date:
2001

ELSEVIER

Materials Science and Engineering A316 (2001) 87–92

MATERIALS SCIENCE & ENGINEERING A

www.elsevier.com/locate/msea

Determination of the Σ 21 [211] orientational relationship in a MgO/Cu composite

Y.G. Wang [a,*], G.H. Yan [b], J.Th.M. De Hosson [c]

[a] *Beijing Laboratory of Electron Microscopy, Institute of Physics and Center for Condensed Matter Physics, Chinese Academy of Sciences, PO Box 2724, Beijing 100080, People's Republic of China*

[b] *Department of Physics, Liaoning University, Shenyang 110036, People's Republic of China*

[c] *Department of Applied Physics, Materials Science Center, University of Groningen, Nijborgh 4, 9747 AG Groningen, Netherlands*

Received 15 June 2000; received in revised form 19 February 2001

Abstract

The microstructure of an internally oxidized CuMg alloy has been examined by means of high-resolution transmission electron microscopy. A new orientational relationship, Σ 21 [211], has been determined by selected-area electron diffraction. The dislocation network for such an orientational relationship, calculated using the near coincident site lattice theory, is a parallel array of edge dislocations with Burgers vectors of the type 1/21[1 0 2 $\bar{1}$], 1/21[1 $\bar{4}$ 2], and 1/21[$\bar{4}$ $\bar{5}$ $\bar{8}$].

Keywords: Internal oxidation; Cu/MgO composite; Dislocation; Transmission electron microscopy

1. Introduction

The importance of interfaces is connected primarily to their inherent inhomogeneity, i.e., the fact that the physical and chemical properties of a material may change dramatically at or near the interfaces. It should be realized that the physical properties, such as the elastic modulus, thermal expansion or electrical resistivity could differ near the interfaces by several orders of magnitude from those of bulk regions. As a result, the sharp gradients may change an isotropic bulk solid locally to a highly anisotropic medium [1–5]. Consequently, many processes are controlled by the interface phenomena such as de-cohesion or segregation. Cavitation and diffusion occur in a very narrow region within a few lattice spacings [6–9], where two materials join. Therefore, the determination of interface orientations as well as the interface planes need be understood in order to establish the physical mechanisms for various boundary phenomena. Experimental techniques capable of revealing the microstructure with atomic resolution are necessary for the investigation. In the present paper, an understanding of the interfaces between copper and magnesium oxide at the atomic level, using high-resolution transmission electron microscopy (HRTEM) as the experimental method will be reported and discussed.

2. Experimental

The copper–magnesium alloy was made with 2.5 atomic percent of Mg in a high frequency oven. The Cu and Mg used were 99.999% pure. Melting and subsequent cooling of the CuMg mixture were performed in a graphite crucible placed inside an evacuated quartz tube. The alloy was homogenized. Flakes of about 1 mm thickness were internally oxidized in a Rhines pack consisting of Cu_2O, Cu, and Al_2O_3 powders [10], roughly in volume ratio of 1:1:1. Sample material and the mixtures were wrapped in a copper foil and internally oxidized in an evacuated quartz tube. The temperature used was 1173 K for about 5 h. After the internal oxidation, the sample was annealed at about 873 K for 3 h and then cooled down slowly to room temperature. HRTEM specimens were made using the standard preparation techniques. Discs of 3 mm diameter were first cut supersonically out of the flakes. The discs were then ground to about 200 μm with abrasive papers

* Corresponding author.

0921-5093/01/$ - see front matter
PII: S0921-5093(01)01229-1

coated with diamonds of different grain sizes, followed by mechanical thinning using a Gatan 656 dimpling system to a thickness less than 10 μm. Finally, the samples were ion-milled to electron transparency using a Gatan 600 dual ion mill system, operated at a low voltage of 4 kV and a low current of 10 μA. The incident angle of argon ion beam was 15° and the specimen was cooled by liquid nitrogen. In order to reduce the degradation of the HRTEM images resulted from ion milling damage at high voltage and the oxide layer on top of the metal foil, the sample was always cleaned with light ion milling for several minutes using a lower current and energy just prior to observation. Fresh surfaces expose after such a processing. This proved to be effective in reducing the noise in the images.

A JEOL-4000EX/II HRTEM with the spherical aberration coefficient of 1 mm and an interpretable point resolution of 0.18 nm, when operated at 400 kV, was used for studying the microstructure of the MgO/Cu composite. All HRTEM images were taken under axial illumination in order to get rid of the misalignments that affect the image contrast.

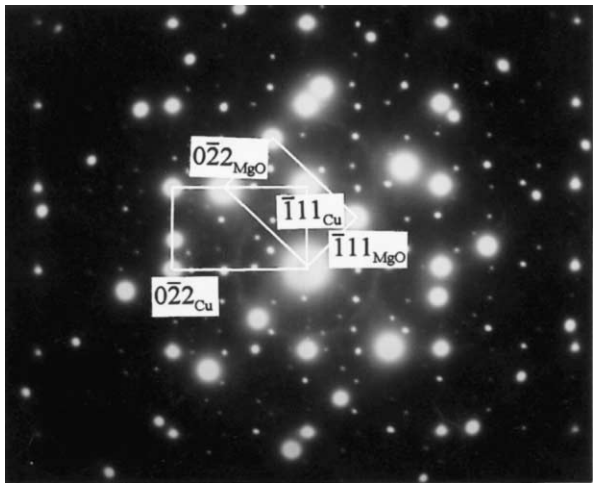

Fig. 1. Composite electron diffraction pattern with the electron beam incident along the common [211] zone axis, showing the 44.41°[211] misorientation between MgO and Cu. The extra spots appear due to double diffraction.

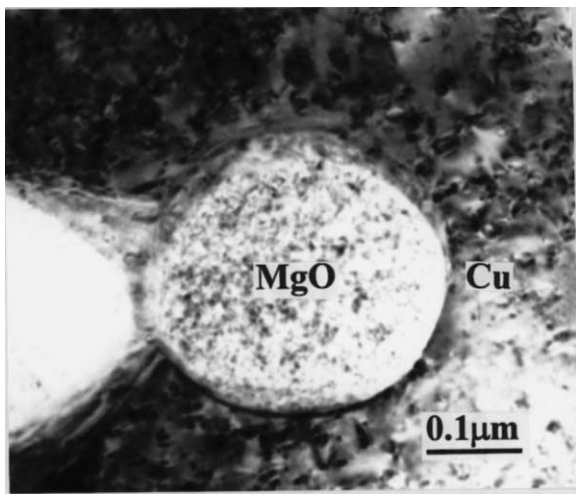

Fig. 2. (a) Bright-field micrograph showing the morphology of a MgO precipitate. A heavily truncated octahedral configuration is suggested for the MgO precipitate. (b) The [211] projection of the truncated octahedron with a ratio of the {100} planes and the {111} planes equal to 1.21.

3. Results and discussion

MgO precipitates form in Cu almost exclusively in a cube-on-cube orientational relationship with the metal matrix. Σ 3 twinning (71°⟨1 1 0⟩) was also observed frequently. Only a few precipitates were found to deviate considerably from the octahedral shape. These precipitates therefore probably had another orientational relationship with the matrix. Fig. 1 is an electron diffraction pattern with the electron beam incident along the common [211] zone axis, showing another orientational relationship. A careful analysis shows that it misorientates by about 44.5° from the cube-on-cube orientation and coincides very well with the Σ 21 [211] orientation [11], which needs a 44.41° rotation around the [211] axis. Due to such a 44.41° [211] rotation, the equivalent planes and directions of Cu and MgO in the cube-on-cube orientation are not parallel. Therefore, their bonding planes may consist of asymmetrical planes. Fig. 2(a) is a bright-field micrograph showing the morphology of a MgO precipitate viewed along the [211] direction. When projected along the [211] direction, a perfect octahedron displays a rectangular configuration. Truncation of all corners could reform the projected shape from a square to a polygon or even an oval, depending on the different ratios of the {1 1 1} planes and the other truncating planes. The most possible sequence of the truncating planes present in the face-centered cubic system is the {1 0 0}, {1 1 0}, and {211} planes. Fig. 2(b) shows a truncated octahedron, projected along the [211] direction, with a ratio of the {1 0 0} planes and the {1 1 1} planes equal to 1.21. A more rounded shape could be obtained if the octahedron were truncated by both the {1 0 0} planes and the {1 1 0} planes. The overlapping contours could be found by the fading image contrast at the top right, left, and the middle bottom parts of the precipitate. It is obvious that the MgO precipitate shown in Fig. 2(a) deviates drastically from an octahedron. Therefore, comparing with Fig. 2(b), it can be suggested that this precipitate were a truncated octahedron with a ratio of the {1 0 0} planes and the {1 1 1} planes around 1.21, between the perfect octahedron and a cuboctahedron, although the corners are not apparent in Fig. 2(a).

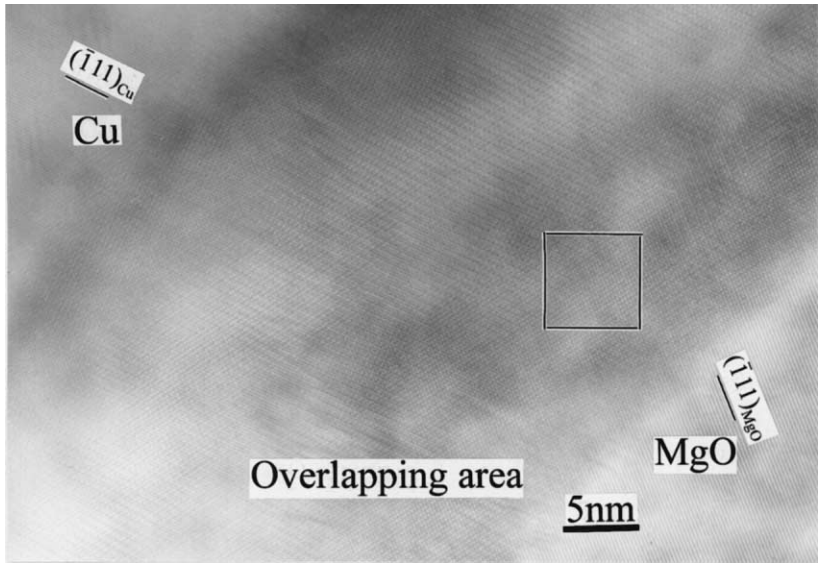

Fig. 3. Low-magnification high-resolution image showing $(\bar{1}\,1\,1)_{Cu}$ and $(\bar{1}\,1\,1)_{MgO}$ fringes as well as Moire fringes in the overlapping area.

With an equal volume, an octahedron has a smaller surface than a cube. However, intermediate shapes, consisting partly of {1 1 1} planes, {1 0 0} planes, and {1 1 0} planes can have a smaller surface area than both the octahedron and the cube. If the interface energy at the {1 0 0} planes and the {1 1 0} planes is higher than that of the {1 1 1} planes, an intermediate shape may still have the interface energy smaller than the perfect octahedron. The shape that minimizes the total interface energy depends on the ratio of these interface energies. However, anisotropic elastic properties may promote certain precipitate shapes and orientations, whereas some growth directions, or mechanisms may be preferred by the kinetics. The occurrence of ledges on the metal-ceramic interfaces as well as the occurrence of flat, elongated precipitates has been interpreted in the past as the signs that these effects may be of importance during growth. Residual thermal stresses are certainly of importance in determining the atomic structure and the metal-oxide interfaces are affected greatly if a large difference of linear expansion coefficients exists between the metal and the oxide. Cu and MgO have nearly the same linear coefficient of thermal expansion, 17 and 14×10^{-6} K^{-1}, respectively, at room temperature, and therefore such an effect could not play any very important role as in a Cu/ZnO system [1].

Viewing along the $\langle 211 \rangle$ direction, the {0 2 2} planar spacings (0.13 and 0.15 nm for Cu and MgO, respectively) are just beyond the resolution of the electron microscope used in this study. The dotted pattern in the high-resolution image can only be made in the overlapping areas, where the Moire effect occurs. Moire effect introduces a complex modulation, which enlarges the planar distance to be resolvable and distorts the relative orientations of the images of adjacent planes. The corresponding high-resolution image taken at the boundary of MgO and Cu is shown in Fig. 3, in which the $(\bar{1}\,1\,1)$ fringes can be identified in the MgO and Cu areas, respectively. Fig. 4 is an enlarged image of the overlapping area, where the image dots are visible. In this figure, the spacing of fringes can be identified to be coincident with the $(\bar{1}\,1\,1)_{Cu}$, $(\bar{1}\,1\,1)_{MgO}$ and $(0\,\bar{1}\,1)_{MgO}$ planar distances, respectively. The $(\bar{1}\,1\,1)_{Cu}$ and $(\bar{1}\,1\,1)_{MgO}$ fringes follow exactly the same orientations of these planes in the Cu matrix and the MgO precipitate. But the fringes coincident with the $(0\,\bar{1}\,1)_{MgO}$ planar spacing are not at a right angle to the $(\bar{1}\,1\,1)_{MgO}$ fringes and deviate from the orientation of the $(0\,\bar{1}\,1)_{MgO}$ planes in the MgO precipitate – obviously

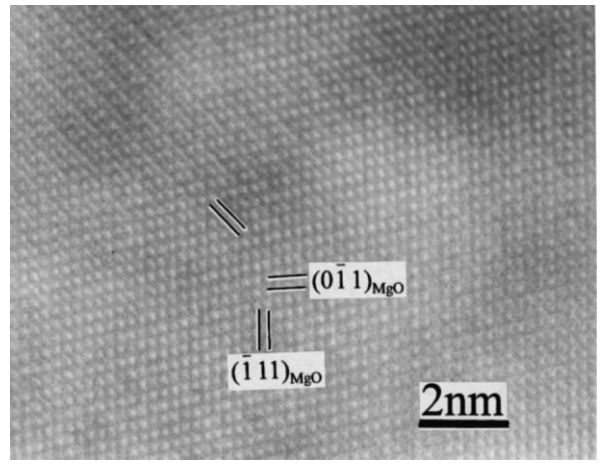

Fig. 4. Enlarged high-resolution image of the marked area in Fig. 3, the $(\bar{1}\,1\,1)_{Cu}$, $(\bar{1}\,1\,1)_{MgO}$ and $(0\,\bar{1}\,1)_{MgO}$ fringes are outlined. The image dots corresponding to the channels surrounded by the Mg, Cu and O atoms due to overlapping of the two structures appear as a result of the Moire effect.

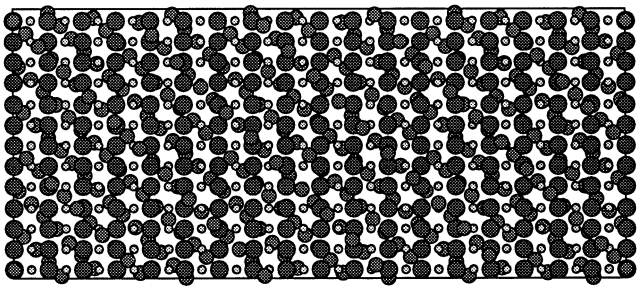

(A)

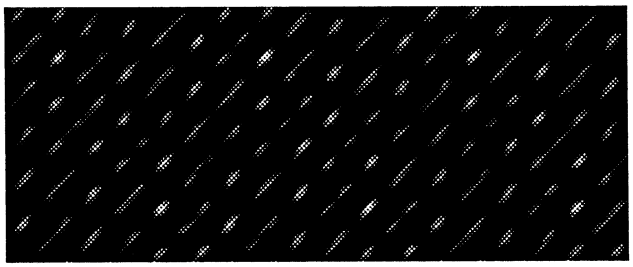

(B)

Fig. 5. (a) A suggested structure model for the 44.41° [211] orientational relationship between MgO and Cu. The large, medium and small circles represent magnesium, copper and oxygen atoms, respectively. (b) A simulated image obtained at thickness of 8 nm and defocusing value of -60 nm. The channels shown in (a) are imaged.

they must be a result of the Moire effect. The Moire pattern, produced by an interference of the discrete reflection beams, forms an displacement site complete (DSC) lattice in the reciprocal space from two overlapped crystals that usually represent the coincident site lattice (CSL) with very large dimensions [15]. In a special case, a Moire pattern may deviate from the CSL pattern and exhibits a high-resolution, especially when the channel pattern constructed from the overlapping of two crystals as shown in Fig. 5(a), where the channel pattern formed as a result of modulation. The $(\bar{1}\,1\,1)_{Cu}$, $(\bar{1}\,1\,1)_{MgO}$, and $(0\,\bar{1}\,1)_{MgO}$ planar spacings can be revealed by the channels within the resolution of the electron microscope. The channels align along both the $(\bar{1}\,1\,1)_{Cu}$ and the $(0\,\bar{1}\,1)_{MgO}$ planar orientations, but the channels result in a distortion of the orientation of the adjacent $(0\,\bar{1}\,1)_{MgO}$ planes. The electron wave might penetrate the two crystals through these channels and gave rise to the channel pattern at the image plane. The $(0\,\bar{1}\,1)_{Cu}$ planar spacing is overwhelmed by the atoms and invisible in the experimental images.

Image simulations have been made in order to interpret the experimental images. A Macintosh Qudra 950 personal computer equipped with the Crystalkit and Mactempas multislice programs developed by Kilaas were used for modeling the complex atomic structure of the Cu/MgO system and the calculation of high-resolution images. The parameters used in the simulations are as follows: spherical aberration coefficient $Cs = 1.0$ mm, beam divergent semi-angle $\theta = 0.50$ mrad, Gaussian defocus spread half-width $\Delta = 5$ nm, and object aperture size $\gamma = 0.09$ nm^{-1}. Fig. 5(a) is a model of overlapping Cu/MgO structures in the 44.41°[211] orientational relationship, in which the Cu atoms close to the interface were relaxed slightly until there is no force larger than 1×10^{-3} eV nm^{-1} on any atom with fitting parameters given in Ref. [16]. The resulting interface seems to be coincident with the semi-coherent one to some extent. The images were simulated basing on this model for both a through-focus series between -25 and -70 nm and a through-thickness series in a range of 3–15 nm. The thicknesses of Cu and MgO used in the calculations were the same. Fig. 5(b) is one of the calculated images obtained at a thickness of 8 nm (both Cu and MgO are 4 nm thick) and a defocusing value of -60 nm. The channels, surrounded by the Cu and Mg metal atoms with the distances coincident with the $(\bar{1}\,1\,1)_{Cu}$, $(\bar{1}\,1\,1)_{MgO}$, and $(0\,\bar{1}\,1)_{MgO}$ spacings, could be imaged clearly under such conditions and match well with the experimental images. The phenomenon of electron channeling is obvious in the present situation.

A matrix **R** relating the two sets of basis vectors for rotating through a 44.41° angle about the [211] zone axis can be obtained [11]

$$\mathbf{R} = 1/21 \begin{pmatrix} 19 & \bar{4} & 8 \\ 8 & 16 & \bar{11} \\ \bar{4} & 13 & 16 \end{pmatrix}. \quad (1)$$

A homogeneous linear transformation matrix **T** relates the metal and the oxide lattice point vectors. The corresponding interface planes in this orientation can be determined using the rotation matrix **R**. In this case, no other pair of planes with low indices in the two crystals is arranged in parallel except the (211) planes. To visualize the structure of the possible misfit dislocation networks at hetero-interfaces, the O-lattice formulation has been widely used [12–14]. The O-lattice is formed by the DSC-1 and the DSC-2 lattices of the Cu matrix and the MgO precipitate. The DSC-1 and the DSC-2 lattices are now the DSC lattices of the Σ 21 [211] misoriented for Cu and MgO, respectively. A basic set of three independent DSC Burgers vectors can be written as

$$\mathbf{B} = (b_1, b_2, b_3) = 1/21 \begin{pmatrix} 10 & 1 & \bar{4} \\ 2 & \bar{4} & \bar{5} \\ \bar{1} & 2 & \bar{8} \end{pmatrix}, \quad (2)$$

where b_1, b_2 and b_3 are the vectors of a primitive unit cell of the DSC lattice in Σ 21 [211] misorientation [11]. Since the transformation matrix **T** between the DSC-1 and DSC-2 lattices is the expansion-contraction matrix **E**, taking Cu as the reference system, the O-lattice point co-ordinates are now given by

$$\mathbf{X}^{(o)} = (\mathbf{I} - \mathbf{E}^{-1})^{-1}\mathbf{B} = (1/\delta)\mathbf{B}, \quad (3)$$

where δ is the lattice mismatch between Cu and MgO defined by

$$\delta = (a_{MgO} - a_{Cu})/a_{MgO}. \quad (4)$$

The O-lattice for this $\Sigma 21$ [211] orientation has a B-face centered orthorhombic structure [11] with lattice constants of $a^{(o)} = (1/\delta)|b_1|$, $b^{(o)} = (1/\delta)|b_2|$, and $c^{(o)} = (1/\delta)|b_3|$. The calculated values of $a^{(o)}$, $b^{(o)}$, and $c^{(o)}$ are ≈ 1.23, 0.55 and 1.23 nm. The three dimensional arrangement of dislocation network consists of three arrays of edge dislocations aligned along the [1 0 2 $\bar{1}$], [1 $\bar{4}$ 2], and [$\bar{4}$ $\bar{5}$ $\bar{8}$] directions individually with Burgers vectors of the type 1/21[1 0 2 $\bar{1}$], 1/21[1 $\bar{4}$ 2], and 1/21[$\bar{4}$ $\bar{5}$ $\bar{8}$]. The spacings between these dislocation lines equal to $a^{(o)}$, $b^{(o)}$, and $c^{(o)}$, respectively. The dislocation structure for (h k l) is obtained by an intersection of the boundary plane with the Wigner–Seitz cell walls of the orthorhombic O-lattice. The resulting dislocation structure of the (211) interface is shown in Fig. 6. Since the [1 0 2 $\bar{1}$] and [$\bar{4}$ $\bar{5}$ $\bar{8}$] directions are out of the (211) plane, the dislocation network of the (211) interface is only one array of edge dislocations aligned along the [1 $\bar{4}$ 2] direction with a Burgers vector of 1/21[1 $\bar{4}$ 2]. The spacing between the dislocation lines is given by

$$Sd = (1/\delta)|b_2|. \quad (5)$$

The calculated value of Sd is 0.55 nm. Because only the $(\bar{1}\ 1\ 1)_{Cu}$ and $(\bar{1}\ 1\ 1)_{Mg}$ planar spacings are resolvable when the electron beam is incident in the [211] direction, it is impossible to measure the mismatch between the corresponding planes of the two structures at the interface in the experimental high-resolution images. The projection of another two arrays of edge dislocations onto the (211) plane should have a periodicity of 0.67 nm.

The origin of DSC lattice shifts to a new origin in the three dimensional space after a displacement of b_1 or b_2 or b_3. Therefore, a property of the DSC vectors is to introduce steps at the interface of the metal and the oxide. The dislocation network predicted by the O-lattice theory is only a geometrical description. Mismatch of the planar spacings at the MgO/Cu interfaces depends on the surface configuration of the MgO precipitates and changes as alternation of the real bonding planes occurs.

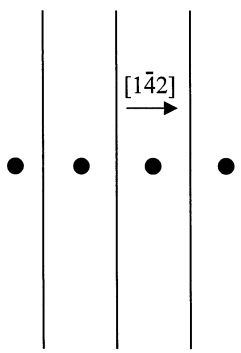

Fig. 6. Schematic drawing showing a dislocation structure on the (211) interface predicted using the O-lattice theory.

An important property of a metal-oxide interface is its free energy per unit area and the closely related work of adhesion. Thermodynamic and mechanical properties of the interface have been found to depend on these parameters. Experimental determination of the interface energy is an important step towards a better understanding of the metal-oxide interfaces. The link between the atomic structure and the interface energy is then provided by the interplay which exists at the interface between the bonding across it and the geometrical misfit that is present. The free energy of the metal-oxide interface is proportional to the square value of the Burgers vector of the misfit dislocations. For the 44.41° [211] misorientation, the scale value of the Burgers vectors of type 1/21[1 $\bar{4}$ 2] is smaller than 1/2$\langle 110 \rangle$ or 1/6$\langle 211 \rangle$, the Burgers vectors for cube-on-cube and the $\Sigma 3$ twinning, respectively [1], the corresponding interfacial energy per unit area contributed by the misfit on the (211) interface is, thus, smaller than those of the above-mentioned orientational relationships. The scale value of 1/21[1 0 2 $\bar{1}$] or 1/21[$\bar{4}$ $\bar{5}$ $\bar{8}$] is smaller than 1/2$\langle 110 \rangle$, but lager than 1/6$\langle 211 \rangle$, therefore, the interfacial energy resulting from the misfit per unit area on the (1 $\bar{4}$ 2) interface is between those for the cube-on-cube and the $\Sigma 3$ twinning orientational relationship. The elastic strain energy and certain facetting accommodated with steps and dislocations also contribute to the total interfacial energy. Because, there is no theoretical data on these energies, it is difficult to compare the interfacial energy between the 44.41° [211] misorientation and the cube-on-cube and the $\Sigma 3$ twinning orientations. Experimentally, the 44.41° [211] misorientation was observed with a much lower frequency than the other two orientations, which implies that such an orientation corresponds to a highest energy among these orientations.

4. Conclusions

Based on the experimental result, it is concluded that the MgO precipitates may deviate considerably from an octahedral shape to assume a configuration between the perfect octahedron and a cuboctahedron in the 44.41° [211] misorientation, though they are often appear in the octahedral or slightly truncated octahedral shapes with the cube-on-cube or the $\Sigma 3$ twinning orientations. Such variations in the surface shape and orientation of the MgO precipitates can minimize significantly the values of the Burgers vectors of the misfit dislocation

network as well as the energy associated with these mismatch dislocations at the bonding planes. To some extent, it may be favorable for the survival of the MgO precipitates with a different orientational relationship with the Cu matrix.

Acknowledgements

Author thanks Dr I. Maclaren, Beijing Laboratory of Electron Microscopy, Chinese Academy of Sciences, and Dr. L.C. Qin, NEC Corporation, for frutiful discussion and review of the manuscript.

References

[1] F. Ernst, Mater. Sci. Eng. R14 (1995) 97.
[2] W. Mader, D. Knaurs, Acta Met. 40 (1992) 207.
[3] V. Vitek, G. Gutekunst, J. Mayer, M. Rühle, Phil. Mag. A71 (1995) 1219.
[4] Y.G. Wang, D. Wang, D.G. Ivey, J. Appl. Phys. 84 (1998) 1310.
[5] D. Duly, W.Z. Zhang, M. Audier, Phil. Mag. A71 (1995) 187.
[6] Z. Zhang, Micros. Res. Tech. 40 (1998) 163.
[7] O.K. Andersen, Z. Pawlowska, O. Jepsen, Phys. Rev. B34 (1986) 5253.
[8] H.X. Zhang, Z.H. Ye, H.M. Lu, B.H. Zhao, Semic. Optoe. 20 (1999) 120.
[9] H.F. Yang, P.D. Han, L.S. Cheng, Z. Zhang, S.K. Duan, X.G. Teng, J. Cryst. Growth 193 (1998) 478.
[10] F.N. Rhines, A.H. Grobe, Trans. AIME 147 (1942) 318.
[11] H. Grimmer, W. Bollmann, D.H. Warrington, Acta Crystal. A30 (1974) 197.
[12] W. Bollman, Crystal Defects and Crystalline Interfaces, Springer, Berlin, 1970.
[13] R. Bonet, F. Durand, Phil. Mag. 32 (1975) 997.
[14] P. Lu, F. Cosandey, Ultramicroscopy 40 (1992) 271.
[15] W. Bollman, Crystal Defects and Crystalline Interfaces, Springer, Berlin, 1970.
[16] G.J. Ackland, G. Tichy, V. Vitek, M.W. Finnis, Phil. Mag. A56 (1987) 735.